Microtubule Assembly of Isotypically Purified Tubulin and Its Mixtures

Vahid Rezania,*† Olga Azarenko,‡ Mary Ann Jordan,‡ Hannes Bolterauer,§ Richard F. Ludueña,¶ J. Torin Huzil,* and Jack A. Tuszynski*

*Department of Oncology, University of Alberta, Edmonton, Alberta, Canada; †Institute for Advanced Studies in Basic Sciences, Zanjan, Iran; ‡Department of Molecular, Cellular and Developmental Biology, University of California, Santa Barbara, California; §Institute of Theoretical Physics, J. Liebig Universitaet Giessen, Giessen, Germany; and ¶Department of Biochemistry, University of Texas Health Science Center, San Antonio, Texas

ABSTRACT Numerous isotypes of the structural protein tubulin have now been characterized in various organisms and their expression offers a plausible explanation for observed differences affecting microtubule function in vivo. While this is an attractive hypothesis, there are only a handful of studies demonstrating a direct influence of tubulin isotype composition on the dynamic properties of microtubules. Here, we present the results of experimental assays on the assembly of microtubules from bovine brain tubulin using purified isotypes at various controlled relative concentrations. A novel data analysis is developed using recursive maps which are shown to be related to the master equation formalism. We have found striking similarities between the three isotypes of bovine tubulin studied in regard to their dynamic instability properties, except for subtle differences in their catastrophe frequencies. When mixtures of tubulin isotypes are analyzed, their nonlinear concentration dependence is modeled and interpreted in terms of lower affinities of tubulin dimers belonging to the same isotype than those that represent different isotypes indicating hitherto unsuspected influences of tubulin dimers on each other within a microtubule. Finally, we investigate the fluctuations in microtubule assembly and disassembly rates and conclude that the inherent rate variability may signify differences in the guanosine-5′-triphosphate composition of the growing and shortening microtubule tips. It is the main objective of this article to develop a quantitative model of tubulin polymerization for individual isotypes and their mixtures. The possible biological significance of the observed differences is addressed.

INTRODUCTION

Microtubules (MTs) are long and relatively rigid hollow protein cylinders that constitute a major component of the cytoskeleton within eukaryotic cells (1). MTs are responsible for several fundamental cellular processes, such as intracellular trafficking, cellular morphogenesis, and cell division. It has also been hypothesized that MTs may be responsible for transferring energy across the cell, with little energy dissipation (2).

MTs are assembled by aggregation of α- and β-tubulin heterodimers in the presence of guanosine-5′-triphosphate (GTP) and magnesium. The irregularity of growing and shortening patterns observed experimentally in MTs may, at first, suggest a very complicated set of processes. In most of the biophysical literature on this topic, two main modes of behavior have been identified and termed: growing and shortening. The implication also made in this context is that these are two distinct dynamical events that somehow compete for the system's involvement. Individual MTs fluctuate stochastically between assembly and disassembly (growing and shortening) phases, in a nonequilibrium process referred to as dynamic instability (3,4). In vitro, only tubulin dimers that are bound to two GTP molecules are assembly-competent; one GTP molecule is bound nonexchangeably to α-tubulin and the other GTP is bound exchangeably to β-tubulin (5). However, upon binding, the exchangeably-bound GTP is rapidly hydrolyzed to guanosine diphosphate (GDP), with the exception of the so-called GTP (or lateral) cap that consists perhaps of only the top layer or two of tubulin dimers (5). It has been speculated that the hydrolysis of GTP weakens lateral and longitudinal tubulin interactions, thereby producing conditions suitable for disassembly. In general, one can summarize MT assembly and disassembly as comprised of the key governing reactions,

1. Generating tubulin-GTP (assembly-competent) (T_{GTP}) from tubulin GDP (assembly incompetent) (T_{GDP}): $\Delta_1 + T_{GDP} \rightarrow T_{GTP}$,
2. Growing of a microtubule: $\Delta_2 + T_{GTP} + MT(n) \rightarrow MT(n+1)$,
3. Shortening of a microtubule: $MT(n) \rightarrow MT(n+1) + \Delta_3 + T_{GTP}$,

where $MT(n)$ is a microtubule with n tubulin dimers, and $\Delta_1 \approx 0.0069$ kcal/mol, $\Delta_2 \approx 0.0017$ kcal/mol, and $\Delta_3 \approx 0.0017$ kcal/mol are the corresponding free energy values given by Caplow et al. (6). The standard designation used in the literature is to refer to the change from a growing phase to a shortening phase as a catastrophe and to its mirror image, i.e., from a shortening phase to a growing phase as a rescue. We note that due to the conversion of tubulin GTP to tubulin GDP after binding to the MT, we did not consider the loss of tubulin GTP as a fundamental process although it most certainly is an intermediate step leading to disassembly. It is also noteworthy that the conformation of growing MTs

Submitted February 25, 2008, and accepted for publication April 22, 2008.

Address reprint requests to Jack A. Tuszynski, E-mail: jtus@phys.ualberta.ca.

Editor: Susan P. Gilbert.

0006-3495/08/08/1993/16 $2.00

doi: 10.1529/biophysj.108.132233

(mainly straight protofilaments) differs from that of shortening ones (with their characteristic curved protofilaments sometimes called the ram's horns) (7,8). This could indicate that polymerization involves the formation of axial interactions while depolymerization consists of breaking lateral bonds already weakened by GTP hydrolysis.

Electron microscopy demonstrated the existence of several stages in the development of a microtubule. An initial nucleation stage from seed oligomers (typically consisting of γ-tubulin in cells) tends to occur slowly reaching an asymptotic density of MT ends after ~1 h (9). This is followed by an almost continuous growth process that is stochastically interrupted by sudden and catastrophic disassembly that can be followed by a growth stage (5,10,11). The average number of nucleated MTs is a nonlinear function of tubulin concentration that increases rapidly above a threshold concentration value. The pattern of growing and shortening is repeated over and over again but seemingly exhibits little regularity. Although it is clear that the dynamic properties of MTs play a significant role in the cell (12,13), little is still known about how their growth is regulated.

Most eukaryotic organisms have multiple genes that encode distinct isoforms or isotypes of α- and β-tubulin. In humans, several isotypes have been identified and characterized (14–16). At the molecular level, the roles and interactions of tubulin are complex and differ between isotypes. For instance, MT dynamics appear to change significantly with β-tubulin isotype composition and MTs constructed from isotypically unfractionated tubulin (IUT) or from purified $\alpha\beta_{II}$ and $\alpha\beta_{IV}$ isotypes are significantly less dynamic than MTs assembled from the $\alpha\beta_{III}$ isotype (14). The availability of high quality structural data for tubulin enabled us, previously, to create comparative models of all currently known α- and β-tubulin isotypes (17). From these results, we have selected, for comparison, the three human β-tubulin isotypes relevant for this study (see Table 1). It is interesting that most of the physical characteristics (charge, dipole moment, volume, surface area) are very similar and would therefore lead us to believe that, contrary to experimental evidence, there should be little difference in the MT assembly kinetics for purified tubulin isotype systems. It has also been demonstrated that, depending upon β-tubulin isotype composition, introduction of paclitaxel to assembly reactions will differentially modulate the dynamicity of MTs. Derry et al. (15) demonstrated that, while there are no significant differences in the mean growing rates of MTs assembled from any of the β-tubulin isotypes, the mean shortening rate of $\alpha\beta_{IV}$ MTs (253 dimers s^{-1}) is significantly lower than the mean shortening rates of $\alpha\beta_{II}$ and $\alpha\beta_{III}$ MTs (343 and 374 dimers s^{-1}, respectively). Furthermore, the mean shortening rate of MTs made from unfractionated tubulin (684 dimers s^{-1}) is much higher than the others (15). These results imply that if MT assembly/disassembly equilibria are disrupted, cells might respond by producing an appropriate isotype mix to restore normal balance. Conversely, a cell could regulate MT dynamic behavior by altering its tubulin isotype composition. While the presence of numerous tubulin isotypes, whose differences are often highly conserved in evolution (18), suggests that they may play specific roles in MT function, there are currently no quantitative models to describe differences between them, let alone describe their behavior in mixtures of isotypes with various concentration ratios.

In this article, we have performed a statistical analysis of MT dynamics occurring in MTs assembled from three isotypically purified β-tubulins to understand how different isotype compositions may affect MT growth and shortening rates. We have then numerically analyzed the differences between the polymerization and depolymerization rates of purified $\alpha\beta_{II}$, $\alpha\beta_{III}$, and $\alpha\beta_{IV}$ MTs. Each of these three isotypes displayed distinct dynamic instability rates. We then developed a simple theoretical model that describes the different growing and shortening behavior of each isotype using a recursive map representation based on a modified random walk model with four independent probabilistic variables describing the possible states of an MT. Using further probabilistic methods, we have performed simulations of the growing and shortening behavior of isotypically pure MTs as well as their mixtures and determined their average growing and shortening rate constants and their probability distributions. The rate constants determined by our model were found to vary significantly between MTs composed of $\alpha\beta_{II}$, $\alpha\beta_{III}$, and $\alpha\beta_{IV}$ isotypes and their mixtures. Finally, we have also investigated the magnitudes of standard deviations in both the growth and shortening rates and deduced from them the plausible energetic substates of the growing tip. Our results indicate that 1), the relationship between the dynamic properties of an isotypically homogeneous MT to the GTP/GDP composition at the tip varies with the isotype; and 2),

TABLE 1 Key biophysical properties of human β-tubulin monomers

Monomer	Name	Dipole moment $\|M\|$ (Debye)	Net charge	Volume (A^{o3})	Area (A^{o2})	C-terminal charge	Tail size	Sequence
β_I	TBB1_HUMAN	2504	−25	43765	46854	−11	19	QDATAEEEEDFGEEAEEEA
β_{II}	TBB1_RAT	3037	−25	43856	46824	−11	20	QDATADEQGEFEEEEGEDEA
β_{III}	TBB4_HUMAN	2494	−25	44223	47074	−11	25	QDATAEEEGEMYEDDEEESEAQGPK
β_{Iva}	TBB2_HUMAN	2311	−25	43874	47064	−11	20	QDATAEEEGEFEEEAEEEVA
β_{IVb}	TBB5_HUMAN	2413	−24	43581	46339	−9	19	QDATAEQGEFEEEAEEEVA

The data reported are from Tuszynski et al. (41).

the dynamic behavior of MTs made of mixtures of isotypes is dependent on specific and hitherto unsuspected isotype-isotype interactions leading to clustering effects.

MATERIALS AND METHODS

Data collection

Data in this article have come from three sources. Two independent sets of data were gathered by digitizing the results published earlier by Panda et al. (14) and Derry et al. (15). The data obtained by Panda et al. presented the time variation in the length of four individual MTs made from purified $\alpha\beta_{II}$, $\alpha\beta_{III}$, or $\alpha\beta_{IV}$ isotypes. Derry et al. (15) reported the time variation in the length of five individual MTs composed from $\alpha\beta_{II}$, $\alpha\beta_{III}$, and $\alpha\beta_{IV}$ isotypes or isotypically unfractioned tubulin. Since the original data presented by Panda et al. (14) and Derry et al. (15) were collected at 2–6 s intervals, the digitized data were collected every 4.2 s. The data were digitized using VistaMetrix (http://www.skillcrest.com/), and sampled into ~200 data points for each trace.

The third source was unpublished results of experiments on MTs (composed of purified $\alpha\beta_{II}$ and $\alpha\beta_{III}$ isotypes from bovine brain tubulin) performed by O. Azarenko, L. Wilson, and M. A. Jordan at the University of California, Santa Barbara. The data acquisition methodology is as follows (see (19) for more detail):

Purification of microtubule protein and tubulin

Microtubule protein preparations consisting of 70% tubulin and 30% MAPs were isolated from bovine brain by three cycles of polymerization and depolymerization. Tubulin was purified from the microtubule protein by phosphocellulose chromatography, drop-frozen in liquid nitrogen, and stored at 70°C (20). On the day of use, the tubulin was thawed on ice and then centrifuged (17,000 × *g*; 20 min; 4°C) to remove aggregated or denatured tubulin. Protein concentration was determined by the Bradford assay using bovine serum albumin as the standard. The isotypically pure tubulin dimers $\alpha\beta_{II}$, $\alpha\beta_{III}$, and $\alpha\beta_{IV}$, were prepared from bovine brain tubulin by immunoaffinity chromatography using monoclonal antibodies to β_{II}, β_{III}, and β_{IV} as previously described (21).

Video microscopy

Purified bovine brain tubulin (15–16 μM) was mixed with sea urchin flagellar axoneme seeds (~1×10^4 seeds/mL) and polymerized in PMME buffer (86 mM PIPES, 36 mM MES, 1 mM EGTA, and 1.4 mM $MgSO_4$, pH 6.8) containing 1 mM GTP for 25–30 min at 37°C. After assembly to polymer mass steady state (~25 min), a 2–3 μl sample was placed between two coverslips and mounted on a prewarmed glass microscope slide. The growing and shortening dynamics of individual MTs at their plus-ends were recorded at 37°C by differential interference contrast video microscopy. Data points representing MT lengths were collected at 2–6 s intervals. MT lengths were analyzed using the Real Time Measurement program, Ver. 5.0 (a kind gift of Neal Gliksman and E. D. Salmon, University of North Carolina, Chapel Hill, NC). Growing and shortening rates were calculated by least-squares regression analysis of the data points for each phase of growth or shortening. A microtubule was considered to be in a growth phase if its length increased by >0.2 μm at a rate of >0.15 μm/min and in a shortening phase if its length decreased by >0.2 μm at a rate of >0.3 μm/min. Length changes ≤0.2 μm over the duration of six data points were considered attenuation phases (phases in which length changes were below the resolution of the microscope). It should be noted that the experimental detection limit for length changes corresponds to ~400–800 tubulin dimers, which is significant for model development and data interpretation.

The supplied data (O. Azarenko, L. Wilson, and M. A. Jordan, unpublished), however, was in the form of a hard copy and we needed to digitize them for our analysis. First the graphs were scanned and then digitized using the software DigitizeIt (http://www.digitizeit.de/). For each graph, we manually set the scale for *x* and *y* axes, clicked on each point, and then exported the data into a comma-separated ASCII text file. We digitized over 30 plots of $\alpha\beta_{II}$ and over 35 graphs of $\alpha\beta_{III}$. The mean and standard deviation analyses are reported in Table 2.

Recursive map model

To provide a simple yet accurate and powerful analysis of the MT assembly data, we use an approach based mainly on recursive maps for the data points, as opposed to the customary representation in the form of a time series, which are typically quite noisy. Appendix A demonstrates how this basic model is directly linked to a more sophisticated but also more complicated master equation representation of the same process. (See Eq. 14 as an example.) The obvious advantage of the recursive maps is the introduction of regularity into the data sets that allows for a better choice of adjustable parameters due to noise reduction inherent in the separation of data into subsets corresponding to independent processes. The second advantage is the simplicity of the mathematical formulas used in simulations. The model presented here possesses sufficient flexibility and can be easily extended to capture a number of subtle features such as: 1), rescue and catastrophe events; 2), nonlinearity effects in the growth process; 3), saturation of growth; and 4), the presence of the attenuation states in both growing and shortening phases that is discussed mathematically in Appendix B. Despite being very simple, recursive map simulations of assembly and disassembly processes of individual MTs presented in this article can successfully reproduce many of the key characteristic features of the experimental data available. Consider first the following stochastic map as the simplest case that illustrates the approach taken,

$$\ell(t_{n+1}) = r(\ell(t_n) + a), \tag{1}$$

where $\ell(t_n)$ is the length of a microtubule after *n* time steps. The difference between the above equation and a deterministic map is that *r* is chosen to be a random number with the following two possibilities:

TABLE 2 Mean ± standard deviation (SD) for $\alpha\beta_{II}$, $\alpha\beta_{III}$, $\alpha\beta_{IV}$, and IUT isotypes

	v^+_{max}	v^+_{min}	v^+_{avg}	v^-_{max}	v^-_{min}	v^-_{avg}	δE_{on}*	δE_{off}*
$\alpha\beta_{II}$ Mean	13.2393	0.3453	3.0828	32.7854	0.3577	5.1577	1.8	1.9
$\alpha\beta_{II}$ SD	7.6265	0.2932	.13006	40.3264	0.2456	2.4384	0.67	0.72
$\alpha\beta_{III}$ Mean	9.1631	0.4233	2.5051	19.8232	0.3974	4.2268	1.5	1.8
$\alpha\beta_{III}$ SD	8.3420	0.4037	1.1276	9.1712	0.3367	1.6010	0.66	0.66
$\alpha\beta_{IV}$ Mean	6.2853	0.0572	1.585	9.6573	0.0657	1.8752	2.3	2.12
$\alpha\beta_{IV}$ SD	2.7423	0.0836	0.5852	7.3922	0.0511	0.6450	0.58	0.50
IUT Mean	9.6558	0.0160	1.0776	18.2900	0.0206	2.0509	2.76	2.9
IUT SD	6.7682	0.0107	0.1006	2.8756	0.0143	0.5849	0.74	0.29

Data are taken from the literature (14,15) and also provided by O. Azarenko, L. Wilson, and M. A. Jordan (unpublished). Velocities are in μm/min.
*Energies are normalized by the free energy of hydrolysis for tubulin-bound GTP, $E_{GTP} \sim 1.2\ k_BT$.

$$\begin{aligned} r &= 1 \quad \text{with probability } p \\ r &= 0 \quad \text{with probability } 1-p. \end{aligned} \tag{2}$$

In terms of the MT polymerization process, p is the probability that a given event will result in assembly, and $1-p$ is the probability of a complete catastrophe of the MT structure. The above simplified model, therefore, is governed by only two adjustable parameters: the probability of complete catastrophe $1-p$ which is constant and independent of the length or time elapsed; and the rate of polymerization which is proportional to the length increment a over the unit of time chosen in the simulation. Thus, the coefficient a divided by the time step Δt ($= t_{n+1} - t_n$) gives the average growth velocity of an individual MT.

In the general case, however, this overly simplistic model requires the probabilities for at least three elementary events that take place stochastically:

1. Catastrophe (with rate f_{cat}) $MT(n) \underset{\text{rescue}}{\overset{\text{catastrophe}}{\rightleftharpoons}} MT(n-m) + mT$,
2. Rescue (with rate f_{res}),
3. Attenuation $MT(n) \rightarrow MT(n)$,

where T represents a tubulin dimer. It is noteworthy that the identification of the attenuation state depends on both temporal and spatial resolutions in measuring the MT length. Here, the spatial resolution is ~400–800 tubulin dimers (~200–400 nm) for the data measured by O. Azarenko, L. Wilson, and M. A. Jordan (unpublished). However, recently Schek et al. (21) performed a series of experiments with a much higher spatial resolution of ~5–10 nm (~10–20 tubulin dimers). In this study, Schek et al. (21) found that the length of an MT continuously undergoes growing and shortening phases with no attenuation (or no apparent pause) observed.

As expected, the mean growth rates increase linearly with the concentration of tubulin (slope $= k_g = 0.17 \pm 0.02$ μm/min/μM (4.6 $\pm$ 0.5 subunits/(s/μM)) and the intercept $k_{-g} = 0.86 \pm 0.53$ μm/min (23 $\pm$ 14 subunits/s)). Thus, the growth rate can be defined as

$$\langle r_g \rangle = k_g[Tb] - k_{-g}, \tag{3}$$

where [Tb] is the molar concentration of the tubulin dimer, k_g is the second order (more precisely: pseudo-first-order) rate constant for the addition of subunits to the (+) ends, and k_{-g} is the first-order (pseudo-zero-order) rate constant for loss of subunits from the (+) ends during the growth phase of MT dynamics.

RESULTS

As stated above, instead of the usual time series representation, we have used a recursive map analysis to conform to the model proposed above. Plotting $\ell(t_{n+1})$ versus $\ell(t_n)$ leads to the emergence of several straight lines on the return map diagram for the $\alpha\beta_{II}$, $\alpha\beta_{III}$, and $\alpha\beta_{IV}$ isotypes, and IUT (see Fig. 4). These straight lines neatly separate various distinct processes taking place over the course of an experiment (e.g., polymerization, catastrophes, rescues, and the attenuation states). All different data sets exhibit subsets of points characterized by slopes whose values are very close to 1.0 indicating that the growth rates are essentially identical for all the isotypes. However, the isotypes differ in their catastrophe frequency and hence, in their overall dynamicity. In short, the general solution of Eq. 1 can be found as

$$\ell(t_n) = r_0 r^n + ra/(1-r),$$

where r_0 is a constant that is determined by the initial conditions. The data were also analyzed to find the maximum, minimum, and mean growth/shortening rates for the purified $\alpha\beta_{II}$, $\alpha\beta_{III}$, and $\alpha\beta_{IV}$ isotypes by finding the average time interval of the corresponding time series. For completeness, the probability distributions for growing and shortening of MTs made from different tubulin isotypes are also presented (see Fig. 3). A note of caution should be made that the different experimental preparations used by us in the analysis lead to significant parameter variations and hence cloud the issue of the absolute values of the model parameters for the individual isotypes. This requires more work to be done in the future on standardization of these data sets. However, it appears that the overall direction of the reported trends is largely reproducible, i.e., $\alpha\beta_{III}$ is generally more dynamic than $\alpha\beta_{II}$ in almost all preparations. Nonetheless, this issue, while not central to the article's key claims, certainly deserves special attention. We discuss the results of our data analysis in more detail in the subsection that follows.

Microtubule assembly data for tubulin isotypes

Fig. 1 represents the variation of the length of a microtubule as a function of time for the $\alpha\beta_{II}$ (Fig. 1 *a*) and $\alpha\beta_{III}$ (Fig. 1 *b*) isotypes. These data were collected from O. Azarenko, L. Wilson, and M. A. Jordan (unpublished). In Fig. 2, we plot the normalized frequency distribution of growing and shortening rates of MTs made from $\alpha\beta_{II}$ (Fig. 2 *a*), $\alpha\beta_{III}$ (Fig. 2 *b*), $\alpha\beta_{IV}$ (Fig. 2 *c*), and unfractionated IUT (Fig. 2 *d*) based on data reported by Panda et al. (14) (*red bars*), Derry et al. (15) (*blue bars*), and collected here (*green bars*). As can be readily seen, the occurrence of the growing/shortening processes as a function of the growing/shortening step size for all tubulin isotypes approximates a normal distribution. The shorter the step size, the higher the probability of the growing/shortening events. This feature can also be seen in Fig. 3 that demonstrates the probability distribution for growing (*left panels*) and shortening (*right panels*) of MTs made from purified $\alpha\beta_{II}$ (Fig. 3, *a* and *b*), $\alpha\beta_{III}$ (Fig. 3, *c* and *d*), $\alpha\beta_{IV}$ (Fig. 3, *e* and *f*) tubulin, and unfractionated IUT (Fig. 3, *g* and *h*), based on the experimental data published in Panda et al. (14) (*pink bars*) and Derry et al. (15) (*blue bars*), respectively. Again the occurrence of a growing/shortening process exhibits a higher probability at a smaller step size and decays more or less exponentially by increasing the step size.

The cumulative recursive maps for the $\alpha\beta_{II}$, $\alpha\beta_{III}$, and $\alpha\beta_{IV}$ isotypes and IUT based on all the data points (growth, attenuation, and shortening) reported in the literature (14,15) and the data of O. Azarenko, L. Wilson, and M. A. Jordan (unpublished) are presented in Fig. 4. The regression analysis of these maps in Fig. 4 for $\alpha\beta_{II}$, $\alpha\beta_{III}$, $\alpha\beta_{IV}$, and IUT demonstrates that all slopes are close to 1 with ~0 intercepts as might be expected from the model. Interestingly, all the different data sets for the three tubulin isotypes have similar slopes and intercepts indicating that the assembly process is largely insensitive to the isotype of tubulin used. However, as noted earlier, the shortening events exhibit a moderate level

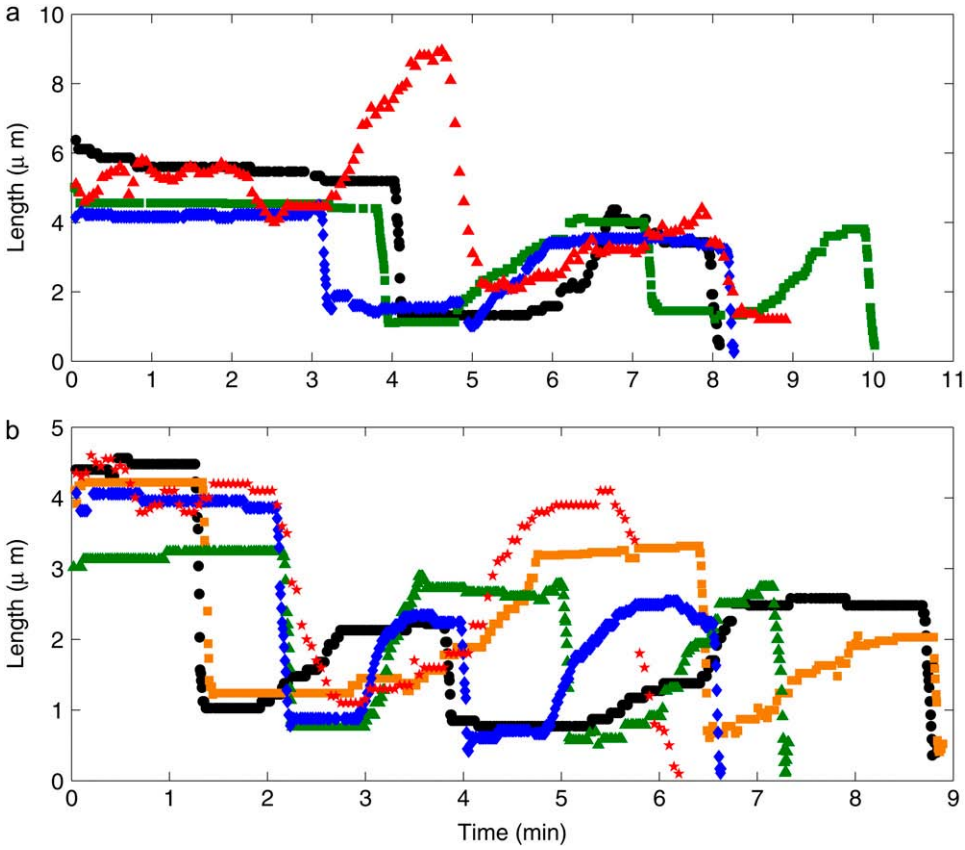

FIGURE 1 Raw data for the selected (*a*) $\alpha\beta_{II}$ and (*b*) $\alpha\beta_{III}$ tubulin isotype measurements performed by O. Azarenko, L. Wilson, and M. A. Jordan (unpublished).

of tubulin isotype sensitivity (see Table 2). The rates of catastrophes and rescues are also moderately dependent on the isotype used (see Table 3). The values for the mean and standard deviation of maximum, minimum, and average rates (in μm/min) of growing and shortening for $\alpha\beta_{II}$, $\alpha\beta_{III}$, $\alpha\beta_{IV}$, and IUT are listed in Table 2. The rates are calculated from the data reported by Panda et al. (14), Derry et al. (15), and the previously unpublished data presented here. Furthermore, we have calculated the values of the associated free energy fluctuations (normalized by the free energy of Δ_{GTP} hydrolysis) during the growing/shortening states using Eqs. 9 and 10. The values for the mean and standard deviation for catastrophes and rescues, respectively, are given in Table 3. The higher values of the standard deviation relative to the mean for the catastrophe events (the opposite is the case for the absolute values of standard deviation) can perhaps be understood due to the lack of observation of this event for individual MTs. The other factor is that the data were derived from different preparations of $\alpha\beta_{II,}$ and $\alpha\beta_{III}$ tubulin made by different investigators over a long period of time. The standard deviation is often not calculated for individual assays since only two, one, or no catastrophes are observed per MT. Finally, the other possible source is that rescues may happen from very fast events (seconds) of variable duration (catastrophes). The variability in catastrophe duration may be greater than the inherent variability in the duration of growth and attenuation phases which go on for minutes.

Table 4 lists the coefficients α and λ for the exponential fit performed, $a\ \exp(-\lambda\ell)$, for the histograms plotted in Fig. 3. We discuss the implications of these growth/shortening rate fluctuations in terms of various substates of the growing MT tips in The Structure of the Microtubule Growing Tip, below.

It is clear from the analysis of these data sets that a faster MT growth is associated with a larger standard deviation in the growth rates. Thus, bringing this discussion to isotype differentiation, the isotypes that grow faster, should also have a larger variability in step size,

$$Q = \mathrm{Var}(r)/\langle r\rangle, \tag{4}$$

where $\mathrm{Var}(r)$ is the variance in the growth or shortening rate, and is approximated as the square of the standard deviation

$$\mathrm{Var}(r) = \sigma^2 = (1/N)\sum_{i=1}^{N}((dn/dt)_i - \langle dn/dt\rangle)^2, \tag{5}$$

where σ is the standard deviation, N is the number of rate values found in a population of datasets used, and n is the number of subunits added to or lost from a microtubule in a given time interval dt. The value of dn/dt is equivalent to r but expressed in the number of subunits per time rather than the length per time. This average intrinsic variability of growth and shortening rates does not change with the rate at which MTs grow. The overall mean values are $Q = 6.0 \pm 1.0$ subunits/s for growth and $Q = 117 \pm 18$ subunits/s for

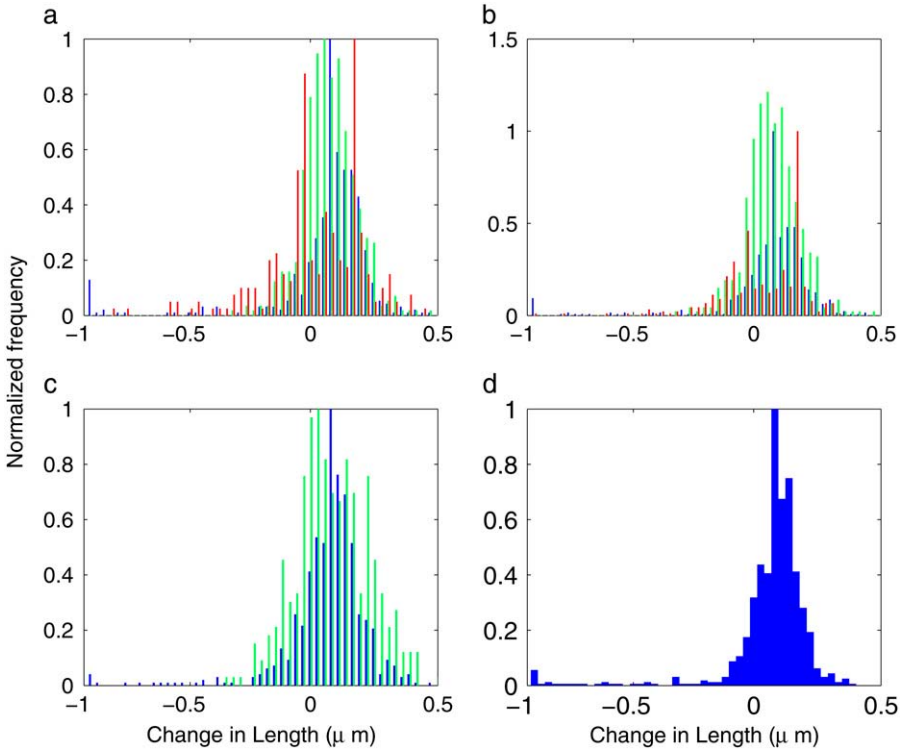

FIGURE 2 Normalized frequency distribution histograms of growing and shortening rates of microtubules made up of (*a*) $\alpha\beta_{II}$, (*b*) $\alpha\beta_{III}$, (*c*) $\alpha\beta_{IV}$ tubulin dimers, and (*d*) unfractionated IUT. Red bars represent the data reported in Panda et al. (14), blue bars represent the data from Derry et al. (15), and green bars refer to the data collected by O. Azarenko, L. Wilson, and M. A. Jordan (unpublished).

shortening. The numbers obtained reveal the shortening processes to be much more variable than the growth processes.

The percentage of time spent by $\alpha\beta_{II}$ and $\alpha\beta_{III}$ MTs in growing, shortening, and attenuation states is demonstrated in Fig. 5. The bars are calculated by averaging over all data. It is clear that, overall, both $\alpha\beta_{II}$ and $\alpha\beta_{III}$ MTs behave dynamically in a similar fashion and the differences, if any, are very subtle.

It is interesting to address the question of the behavior of tubulin isotype mixtures. We have thus far only discussed purified tubulin isotype assembly/disassembly processes and one might naively expect that mixing them together will lead

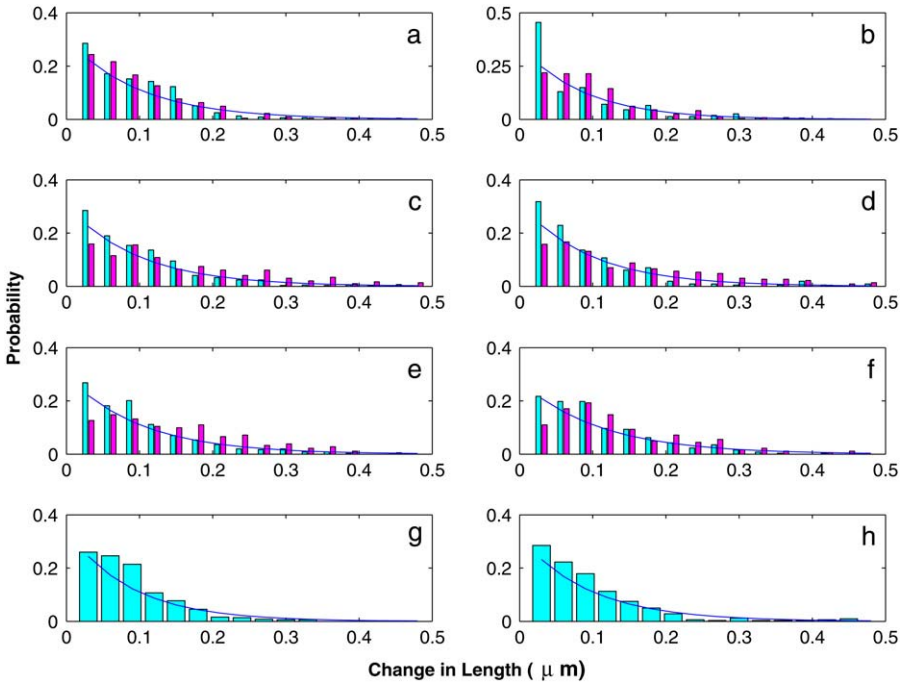

FIGURE 3 The probability distribution function for growth (*left panels*) and shortening (*right panels*) of MTs made up of purified $\alpha\beta_{II}$ (*a* and *b*), $\alpha\beta_{III}$ (*c* and *d*), $\alpha\beta_{IV}$ (*e* and *f*) tubulin, and unfractionated IUT (*g* and *h*). Pink bars correspond to the data from Panda et al. (14) and blue bars are based on the observations in Derry et al. (15). An exponential fit, $a\exp(-\lambda\ell)$, is also shown where coefficients a and λ are given in Table 5.

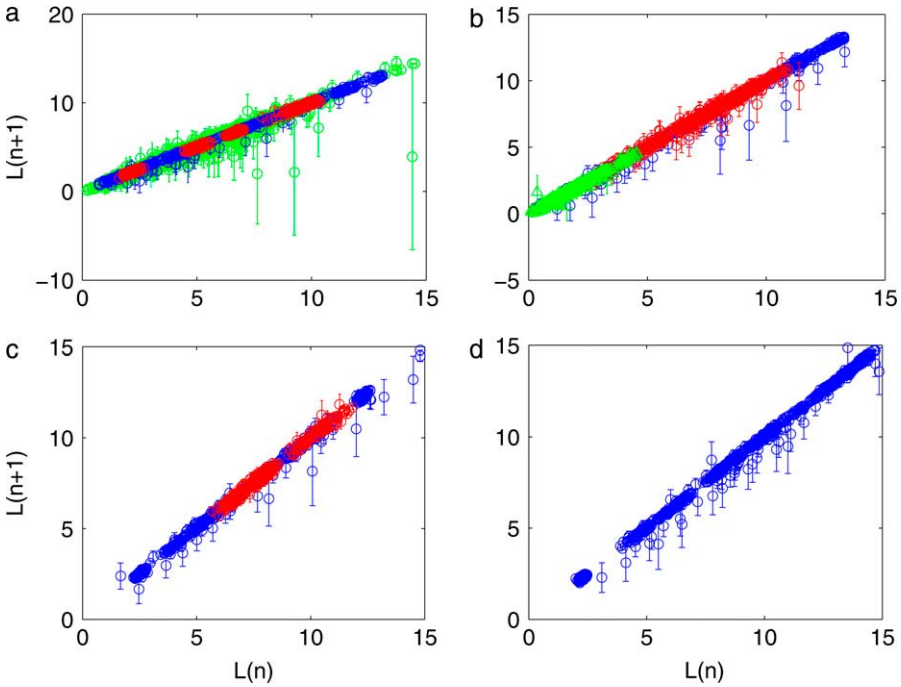

FIGURE 4 Recursive plots for purified (*a*) $\alpha\beta_{II}$, (*b*) $\alpha\beta_{III}$, (*c*) $\alpha\beta_{IV}$ tubulin, and (*d*) IUT based on the data reported by Panda et al. (14) (shown with *red circles*), Derry et al. (15) (shown with *blue circles*), and the data by O. Azarenko, L. Wilson, and M. A. Jordan (unpublished; shown with *green circles*). The slopes and intercepts for different data sets are given in Table 4.

to statistically weighted averages of the measured rates for the various kinetic rates. The section that follows demonstrates that the naive expectation is, in fact, incorrect and that nonlinear effects are observed that give us clues regarding the interactions between different tubulin isotypes in a mixture.

Isotype interactions: $\alpha\beta_{II}$ with $\alpha\beta_{III}$

Panda et al. (14) studied the dynamicity of a mixed $\alpha\beta_{II}/\alpha\beta_{III}$ tubulin solution with different proportions. Surprisingly, they found that the dynamicity of the solution initially decreases with increasing $\alpha\beta_{III}$ proportion, reaches a minimum, and then increases with addition of more $\alpha\beta_{III}$ tubulin to the solution. They observed that the lowest amount of dynamicity occurred when the proportion of $\alpha\beta_{III}$ is 20% of the solution (80% for $\alpha\beta_{II}$). Based on the results of Panda et al. (14), $\alpha\beta_{III}$ is more dynamic compared with $\alpha\beta_{II}$; but, when small amounts of $\alpha\beta_{III}$ are added to a pure sample of $\alpha\beta_{II}$, the dynamicity of the MTs unexpectedly decreases (14). It is known that, for a pure tubulin solution, the growth rate of MTs linearly increases with increasing concentrations (i.e., the first-order interaction). However, this may not be true when two or more isotypes are present in the solution as reported by Panda et al. (14). Therefore, one may need to consider the second- or higher-order interaction between dynamicity and isotype proportions.

TABLE 3 Catastrophe and rescue frequencies for $\alpha\beta_{II}$ and $\alpha\beta_{III}$ obtained from different data sets

	$\alpha\beta_{II}$	$\alpha\beta_{III}$
Catastrophe frequency (min^{-1})		
Panda et al. (14)	1.2	1.5
Derry et al. (15)	0.18	0.27
O. Azarenko, L. Wilson, and M. A. Jordan (unpublished)	0.4	0.37
Mean ± SD	0.46 ± 0.39	0.56 ± 0.49
Rescue frequency (min^{-1})		
Panda et al. (14)	3.3	2.2
Derry et al. (15)	3.2	4
O. Azarenko, L. Wilson, and M. A. Jordan (unpublished)	1.9	2
Mean ± SD	2.83 ± 0.61	3.17 ± 0.87

The mean ± SDs are calibrated by the number of MTs used in the respective measurements: 33 MTs used by Panda et al. (14); 14 MTs used by Derry et al. (15); and 20 MTs used by O. Azarenko, L. Wilson, and M. A. Jordan (unpublished).

For example, a second-order interaction can be easily examined by fitting the second-order polynomial through the data

$$y(c_{II}) = ac_{II}c_{III} + bc_{II} + c;\ c_{II} + c_{III} = 1,$$
$$y(c_{II}) = y_2c_{II}^2 + y_1c_{II} + y_0, \quad (6)$$

where $y_2 = -a$, $y_1 = (a + b)$, and $y_0 = c$ are the constants that can be determined by curve fitting over the data. Here, $y(c_{II})$ represents the dynamicity/inverse attenuation variance of $\alpha\beta_{II}$, and c_{II} and c_{III} are the proportions of $\alpha\beta_{II}$ and $\alpha\beta_{III}$, respectively. The parameters describing the second-order interactions between $\alpha\beta_{II}$ and $\alpha\beta_{III}$ are calculated in Table 5. On its own, $\alpha\beta_{III}$ is clearly very dynamic and spends very little time in an attenuated state, and $\alpha\beta_{II}$ is much less dynamic and spends a greater amount of its overall time pausing when pure isotype samples are measured. As shown by Panda et al. (14), adding 20% of a very dynamic isotype, $\alpha\beta_{III}$, actually decreases the dynamicity of the overall sam-

TABLE 4 The coefficients of exponential fits, $a \exp(-\lambda \ell)$, based on the histograms in Fig. 3

	Growing		Shortening		Regression analysis*		
Isotype	a	λ	a	λ	Slope	Intercept	Data
$\alpha\beta_{II}$	0.3047	10.16	0.3508	11.69	0.9996	0.0008	Panda et al. (14)
					1.0014	−0.0244	Derry et al. (15)
					0.9999	−0.0184	O. Azarenko, L. Wilson, and M. A. Jordan, unpublished
$\alpha\beta_{III}$	0.3047	10.16	0.3138	10.46	0.9964	0.0300	Panda et al. (14)
					0.9970	−7.0E-5	Derry et al. (15)
					0.9955	0.0002	O. Azarenko, L. Wilson, and M. A. Jordan, unpublished
$\alpha\beta_{IV}$	0.2961	9.87	0.2753	9.178	0.9948	0.0520	Panda et al. (14)
					0.9942	0.0315	Derry et al. (15)
IUT	0.3445	11.48	0.3187	10.62	1.0008	−0.0167	Derry et al. (15)

*Regression analysis of the recursive maps plotted in Fig. 4.

ple, and then with increasing amounts of $\alpha\beta_{III}$, the dynamicity falls closer to what we would intuitively expect. To explain the behavior at lower $\alpha\beta_{III}$ proportions though, we need to reexamine certain assumptions.

It is interesting to note that unfractionated (isotypically heterogeneous) tubulin was previously shown to be the slowest to polymerize, while $\alpha\beta_{III}$ was the fastest (22). It is worth noting that the purified isotypes polymerize faster than the IUT (unpurified mixture), which shows that the assembly rate of the IUT is not simply an average of the dynamic rates of the component isotypes. From these results, it appears obvious that there are other uncharacterized interactions taking place. It is possible that there are higher-order interactions between tubulin dimers of different isotypes, leading to a more complex interaction and thereby slowing down the overall polymerization process. Below we present our hypothesis that aims at clarifying this picture.

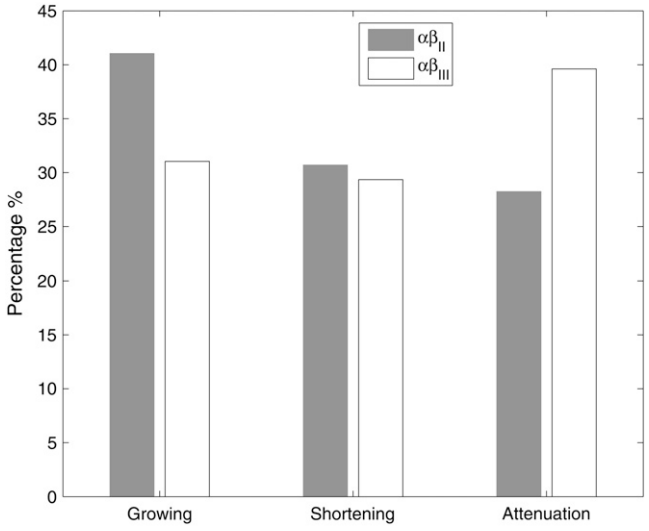

FIGURE 5 Overall percentage of time spent by a microtubule in the growing, shortening, or attenuation states. The bars are calculated by averaging over all the data.

Clustering

As mentioned above, the unusual aspect of the results reported by Panda et al. (14) is that when $\alpha\beta_{II}$ and $\alpha\beta_{III}$ dimers are mixed, the presumably isotypically heterogeneous MTs that result are significantly less dynamic than those formed from either $\alpha\beta_{I}$ or $\alpha\beta_{II}$. This is somewhat counterintuitive since one would expect the mixture to have a dynamicity intermediate between those of $\alpha\beta_{II}$ and $\alpha\beta_{III}$. These results could be explained if one assumes that the individual dimers can influence each other's dynamic behavior. A possible model assumes that the affinity between an $\alpha\beta_{II}$ and an $\alpha\beta_{III}$ dimer is greater than that between either two $\alpha\beta_{II}$ dimers or two $\alpha\beta_{III}$ dimers. The corollary to this assumption is that an individual $\alpha\beta_{III}$ dimer would form a cluster in the MT (initially at its growing tip due to an increased affinity for binding) with several $\alpha\beta_{II}$ dimers in its vicinity. Such behavior is schematically shown in Fig. 6 *a*, where the newly arriving $\alpha\beta_{II}$ dimer has a higher propensity to polymerize into an MT next to an assembled $\alpha\beta_{III}$ tubulin dimer rather than an $\alpha\beta_{II}$ dimer. Similar behavior is also expected for a newly arriving $\alpha\beta_{III}$ dimer that prefers to polymerize directly next to an $\alpha\beta_{II}$ tubulin dimer. Compared to pure $\alpha\beta_{II}$ and $\alpha\beta_{III}$ isotypes, this new type of competition between $\alpha\beta_{II}$ and $\alpha\beta_{III}$ would affect the MT's growing/shortening processes and hence the overall dynamicity of MTs would decrease. Fig. 6 *b* schematically represents the potential barrier between assembled (A) and free (F) states of $\alpha\beta_{II}$-$\alpha\beta_{II}$, $\alpha\beta_{III}$-$\alpha\beta_{III}$, and $\alpha\beta_{II}$-$\alpha\beta_{III}$ structures based on the observations made by Panda et al. (14) and our interpretation put forward above.

TABLE 5 The parameters describing the second-order interactions between $\alpha\beta_{II}$ and $\alpha\beta_{III}$ tubulin isotypes

	y_2	y_1	y_0
Coefficients for dynamicity variance	0.0064	−0.1631	24.2676
Coefficients for inverse attenuation variance	0.0004	−0.0148	2.0001

See Eq. 6 for detail.

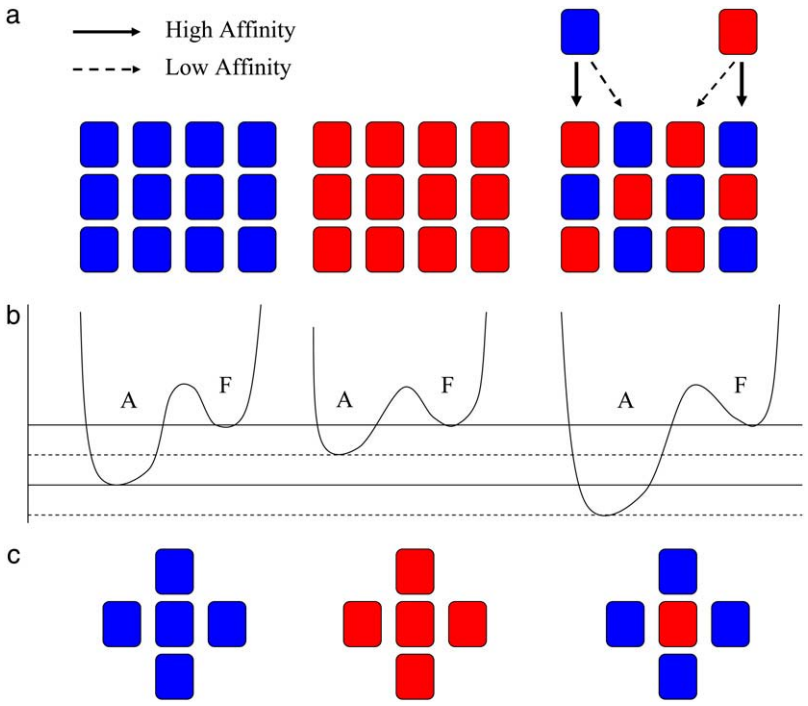

FIGURE 6 Schematic representation of MTs made up of the purified $\alpha\beta_{II}$ (*blue squares*) and $\alpha\beta_{III}$ (*red squares*) tubulin and mixtures of $\alpha\beta_{II}$ and $\alpha\beta_{III}$. (*a*) It is assumed that the affinity between an $\alpha\beta_{II}$ and an $\alpha\beta_{III}$ dimer is greater than that between either two $\alpha\beta_{II}$ dimers or two $\alpha\beta_{III}$ dimers. As a result, an MT made up of mixed isotypes has a more stable assembled structure than that of isotypically purified MTs. This is shown in panel *b* where the potential barrier between the assembled state (*A*) and the free tubulin state (*F*) is deeper for the mixed structure. The $\alpha\beta_{III}$ MT has a smaller potential barrier based on the observations made by Panda et al. (14). (*c*) The simplest possible sublattice for purified and mixed MTs.

Consider now a microtubule made up of only $\alpha\beta_{II}$ dimers in a solution consisting of purified $\alpha\beta_{II}$ tubulin. Now add a small amount of $\alpha\beta_{III}$ isotype to the solution. The newly added $\alpha\beta_{III}$ dimers will compete with existing free $\alpha\beta_{II}$ dimers for their assembly into the MT. As a result, a number of $\alpha\beta_{III}$ (say n) will be polymerized into the MT. Such competition will reduce the concentration of free $\alpha\beta_{III}$ dimers in the vicinity of the MT. Furthermore, m ($>n$) number of $\alpha\beta_{II}$ dimers will prefer to assemble around $\alpha\beta_{III}$ dimers. Due to the higher affinity between $\alpha\beta_{II}$ and $\alpha\beta_{III}$ dimers, the newly assembled MT is more stable structurally and hence less dynamic than isotypically purified MTs (see Fig. 6 *b*). The percentage of the total time that the mixture spends in growing, shortening, and attenuation can be calculated by

$$\begin{aligned} p &= N_{II}p_{II} + N_{III}p_{III} + N_{cl}p_{cl}, \\ q &= N_{II}q_{II} + N_{III}q_{III} + N_{cl}q_{cl}, \\ r &= N_{II}r_{II} + N_{III}r_{III} + N_{cl}r_{cl}, \end{aligned} \tag{7}$$

where p, q, and r are the overall probabilities of growing, shortening and the attenuation states, respectively, for the newly assembled MT. N_{II}, N_{III}, and N_{cl} represent the number of $\alpha\beta_{II}$-$\alpha\beta_{II}$, $\alpha\beta_{III}$-$\alpha\beta_{III}$, and $\alpha\beta_{II}$-$\alpha\beta_{III}$ sublattices. The geometrically simplest structure for a sublattice is to assume that one dimer at the center is surrounded by four either similar or different dimers (Fig. 6 *c*). We numerically reproduced the Panda et al. (14) results for the mixed sublattice by choosing $m/n \sim 3.6$, p_{cl}: 0.2, q_{cl}: 0.2, and r_{cl}: 0.6. The value $m/n \sim 3.6$ represents, for each $\alpha\beta_{III}$ dimer, that approximately four $\alpha\beta_{II}$ dimers are needed (as expected). The values of p, q, and r for $\alpha\beta_{II}$ and $\alpha\beta_{III}$ are given by Panda et al. (14). To reproduce the dynamicity results, we also assumed that the mean rate for both growing and shortening of the clusters is $\approx 30\ s^{-1}$. This is illustrated in Fig. 7 where white bars show the concentration dependence of dynamicity while gray bars represent the percentage of total time that the MTs spent in the attenuated state for a mixed $\alpha\beta_{II}/\alpha\beta_{III}$ solution. Bars are calculated based on the clustering model. The squares and diamonds represent the corresponding experimental values reported by Panda et al.

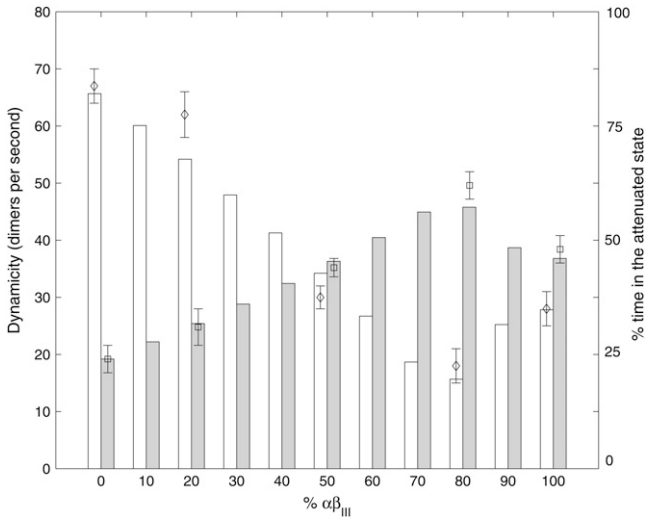

FIGURE 7 Concentration dependence of dynamicity (*white bars*) and the percentage of total time that MTs spent in the attenuated state (*gray bars*) for a mixed $\alpha\beta_{II}/\alpha\beta_{III}$ solution. Bars are calculated based on the clustering model. The squares and diamonds represent the experimental values reported by Panda et al. (14).

(14). The above rationale, therefore, is consistent with the experimental observations of a nonlinear dependence of the dynamicity data on the concentration of one isotype in a mixture. This nonlinear behavior can be explained by the existence of different affinities between tubulin dimers. More specifically, during the MT assembly process, different isotypes have a stronger affinity for forming clusters with each other than do identical isotypes. It is also possible that one dimer induces conformational changes that affect other dimers including possibly dimers that are not immediately adjacent to the first one. Interestingly, binding of other proteins, such as motors, to the MT, could be spaced as a result of this conformational change. Such a phenomenon was first proposed for the heliozoan axopodium in 1970 by Roth et al. (23) and elaborated further in 1977 (24). These authors termed this the ''gradion model,'' which postulates that a ligand binding to one tubulin molecule in a microtubule could cause a graded conformational change that would inhibit binding of another molecule of that ligand to adjacent tubulin molecules. The change would dissipate with increasing distance from the ligand, allowing a tubulin molecule at an appropriate distance from the first one to bind to another molecule of that ligand as well. In other words, there would be even spacing among the ligand molecules. Our results are consistent with such a model. In practical terms, the β_{II}, β_{IVa}, β_{Ivb}, and β_{I} isotypes may be too similar to each other to exhibit very complex clustering properties (although this has not yet been tested), so cells whose tubulin expression is limited to these isotypes may not exhibit the effects of clustering that we have hypothesized. However, the structural differences between these isotypes, on the one hand, and β_{III} and β_{V}, on the other hand, are substantially greater and cells containing at least one of the latter two isotypes as well as some of the former would show clustering and may indeed exhibit the hypothesized effects. We conclude that it is plausible that different isotypes tend to form clusters that result in a marked decrease in the average dynamicity of the mixture.

The structure of the microtubule growing tip

We have also applied our analysis to the structure of the MT's growing tip in the case of different tubulin isotypes. Previous studies focused on analyzing the length and time histograms for MTs to shed light on their statistical properties that are presumed to be related to structural characteristics of MTs. For example, a histogram of delays before catastrophes for both ends has a characteristic Poissonian shape, suggesting statistically independent, small probability events. On the basis of an inverse proportionality of the frequency of catastrophes to the growth velocity of a microtubule, it has been concluded that a GTP cap exists at the growing end of a microtubule (25). In addition, Panda et al. (26) determined the size and chemical nature of the lateral cap biochemically. It is generally believed that a rate of GTP supply exceeding that of the internal hydrolysis processes stabilizes a growing phase of an MT. Odde et al. (27) analyzed the distribution of growth times and found that while the minus-end histograms are exponential in character, the plus-end counterparts are not. This would mean that the effective catastrophe frequency for minus-ends is independent of the length of the growth phase. On the other hand, for the plus-end, it increases with the growth period reaching eventually a saturation value. These conclusions may lead to more accurate models of MT assembly that account for nonlinear properties and possibly memory effects (see Appendix B for some simple extensions of the basic model that account for such possibilities).

It has also been suggested that there are inherent fluctuations in the growing and shortening rates of MTs that cannot be attributed to the variations in the number of protofilaments or defects in the structure (28). We propose an explanation of this inherent rate variability that has also been seen in all the assembly data sets studied in this article. In fact, because the data presented here pertain to individual MTs, the variability is even greater. Our main assumption is that the growth and shortening fluctuations are due to the possibility of diverse structures at the tip of a growing/shortening state of a microtubule. These possibilities can be viewed as distinct manifestations of a statistical macrostate (growth, shortening, attenuation) in terms of microstates or substates that, although may not resolved experimentally, can be deduced theoretically to offer a consistent interpretation, as we attempt below. The differences between the structures of growing tips may be viewed in terms of the GTP/GDP composition at the exchangeable sites (which is our assumption), or due to other structural features such as the presence of defects, protrusions, etc. All of these differences are clearly physically possible and the question that can be posed is, how will they be manifested through measurable properties of MTs? We advance the hypothesis that the main difference between the various microstates characterizing a growing (or shortening) tip can be linked to the free energy stored at the tip. One key consequence of it is the difference in the potential energy barrier separating the assembled tubulin (MT structure) from the free state of tubulin in solution that can be linked to the on- and off-rates for the polymerization processes that vary according to

$$k_{on} \sim e^{-\Delta E_{on}/k_B T}, \qquad k_{off} \sim e^{-\Delta E_{off}/k_B T}, \tag{8}$$

where k_B is the Boltzmann constant. Fig. 8 illustrates these differences graphically in more detail by showing how the different GTP/GDP states of exposed tubulin relate to the free energy differences which, in turn, relate to the on- and off-rates according to the Arrhenius relation. Fluctuations in $\Delta E_{on/off}$, i.e., $\Delta E_{on/off} \pm \delta E_{on/off}$, cause the on/off-rate fluctuations between maximum and minimum rates $k_{max/min}$: $k \pm \delta k$. As a result, by measuring the maximum and minimum rates of growing/shortening state, one can find $\delta E_{on/off}$ as

$$\delta E_{on} = 0.5\, k_B T \ln\left(\frac{k_{on}^{max}}{k_{on}^{min}}\right), \tag{9}$$

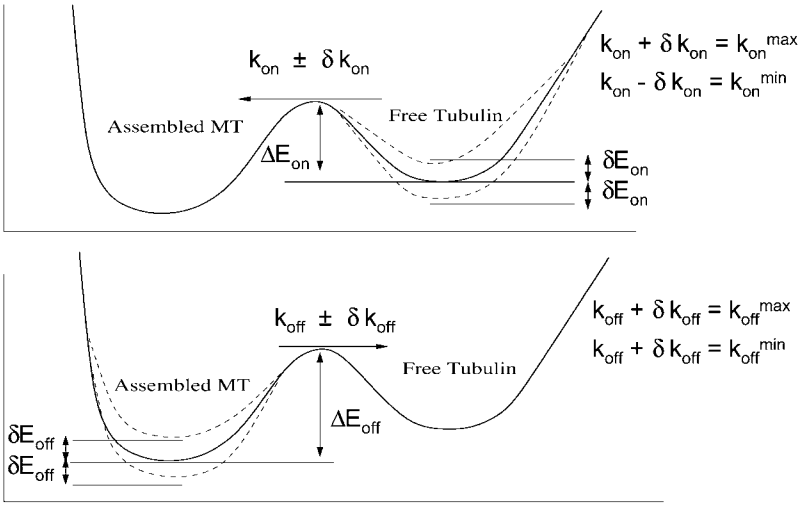

FIGURE 8 Schematic representation of the potential barrier between an assembled MT and free tubulin at the plus-end (*upper panel*) and minus-end (*lower panel*). The values k_{on} and k_{off} represent association and dissociation rates related to the free energies ΔE_{on} and ΔE_{off}. The possible fluctuations in the free energies, δE_{on} and δE_{off}, increase or decrease the association and dissociation rates, respectively, as per the Arrhenius relationship.

$$\delta E_{off} = 0.5\, k_B T \ln\left(\frac{k_{off}^{max}}{k_{off}^{min}}\right), \tag{10}$$

when in a microtubule structure, the free energy of hydrolysis for tubulin-bound GTP is $E_{GTP} \sim 1.2\ k_B T$ (6). In Table 2 using the calculated maximum and minimum growing and shortening rates, the fluctuations in the free energy of hydrolysis $\delta E_{on/off}$ in units of E_{GTP} are obtained for each sample. We see through this analysis that the MTs composed of $\alpha\beta_{II}$ and $\alpha\beta_{IV}$ isotypes could have growing tips with 13, 12, 11, 10, 9, or even 8 GTP molecules at their exchangeable sites (for a maximum difference of five free energies of GTP hydrolysis) while the growing MT composed of the $\alpha\beta_{III}$ isotype tubulin can have a tip with between 13 and 9 GTP molecules. On the other hand, the shortening tips for MTs composed of $\alpha\beta_{II}$ and $\alpha\beta_{IV}$ tubulin isotypes may contain between 0 and 4 GTP molecules while the MTs composed of $\alpha\beta_{III}$ tubulin allow for an extra GTP molecule for a range between 0 and 5 GTP molecules. The values in between, i.e., 5–7 GTP molecules for MTs composed of $\alpha\beta_{II}$ and $\alpha\beta_{IV}$ tubulin and from 6 to 8 GTP molecules for MTs composed of $\alpha\beta_{III}$ tubulin, can be interpreted as giving rise to an attenuation state. Table 2 also summarizes the data for IUT wherefrom we could conclude that its growing tip has between 13 and 7 and a shortening tip between 0 and 6 GTP molecules in the exchangeable sites, allowing for very little in terms of an attenuated state.

DISCUSSION

Microtubule polymerization and especially depolymerization processes are fairly complex and many of their aspects are still incompletely understood at a microscopic level (28–33). The geometry of a microtubule lattice is a separate issue and has been discussed in a review article (34). The rate of MT polymerization depends crucially on the concentrations of tubulin, GTP, and ionic species (35). Tubulin subunits form a regular array but each MT is anisotropic, i.e., it has two ends that behave differently with respect to growing and shortening characteristics, namely the plus-end grows faster while the minus-end grows more slowly.

In the dynamic instability phenomenon (3), the rates at which the assembly and disassembly processes for MTs occur are quite different. The rate of disassembly is typically 10–20 times faster than the rate of growth. This has been seen both in vivo and in vitro (7,8,36). The rate of growth for both the plus- and minus-ends increases almost linearly with tubulin concentration (37). Furthermore, the slope of each growth curve increases with magnesium concentration. On the other hand, the frequency of catastrophes appears to be virtually independent of the tubulin concentration in the solution for both plus- and minus-ends although some authors detected a linear decrease of catastrophe frequencies with the amount of tubulin available (38). The frequency of rescues has been found to be almost linearly proportional to the tubulin concentration for both ends (25,38).

Various studies focused on analyzing histograms for MTs to shed light on their statistical properties. For example, a histogram of delays before catastrophes for both ends has a characteristic Poissonian shape that is suggestive of statistically independent, small probability events. Histograms illustrating length distributions have an exponential long tail and a peak corresponding to relatively short MTs, again in analogy to Poissonian processes. On the basis of an inverse proportionality of the frequency of catastrophes to the growth velocity of an MT, an important conclusion was reached—that it indicates the presence of a GTP cap at the growing end. In addition, we know that GTP-tubulin has a higher affinity for the MT end than GDP-tubulin, and GTP has a higher affinity for tubulin than GDP. We also know that a cap of GDP-Pi is found at the end of MTs in the experiments of Panda et al. (26), even several hours after they have been removed from the GTP-containing buffer and sedimented

through a sucrose cushion. Thus, it is not sufficient to conclude that the GTP supply exceeding the internal hydrolysis process stabilizes a growing MT. We must conclude that there is a persistent biochemical cap.

Odde et al. (27) investigated the validity of the standard assumption that the growing and shortening of MTs is governed by first-order chemical kinetics. They analyzed the distribution of growth times and found that while the minus-end histograms are exponential in character, the plus-end counterparts are not. This would mean that the effective catastrophe frequency for minus-ends is independent of the length of the growth phase. On the other hand, for the plus-end, it increases with the growth period reaching eventually a saturation value. Time series for growing and shortening MTs may appear to indicate the presence of. an attenuation state in the midst of both elongation and shortening periods. However, we feel that it is important to note that attenuation is not really a distinct state, but rather a period of time during which we cannot experimentally discern whether a MT is growing or shortening due to the inadequate resolution of the method used.

As discussed above, Panda et al. (14) showed experimentally that the dynamics of $\alpha\beta_{III}$ MTs will change after adding the $\alpha\beta_{II}$ isotype along with the $\alpha\beta_{III}$ isotype in the solution during polymerization. They examined a mixture of $\alpha\beta_{II}$ and $\alpha\beta_{III}$ tubulin isotypes at three different ratios: 20:80, 50:50, and 80:20%, respectively. As shown in Fig. 7, the dynamicity as well as the percent of time spent in the attenuation state of the $\alpha\beta_{II}$ and $\alpha\beta_{III}$ mixture shows a nonlinear behavior. Here, we fit the observed data with a second-order function of $\alpha\beta_{II}$ tubulin proportion, c_{II}. The parameters are listed in Table 5. We explained this nonlinear interaction of $\alpha\beta_{II}$ and $\alpha\beta_{III}$ isotypes due to the clustering of the isotypes together. We showed that a cluster of 3–4 $\alpha\beta_{II}$ tubulin dimers surrounding one $\alpha\beta_{III}$ tubulin dimer can describe the observed nonlinear behavior in the MT dynamicity (see Fig. 6 for illustration).

We have seen through the analysis of the data presented in this article that different tubulin isotypes differ in regard to their polymerization properties when forming MTs. This is especially true of catastrophe frequencies. With very little in terms of biophysical differences between them, as discussed earlier in the article we wish to compare their structural properties in more detail, especially in regard to the dimer/dimer contacts that are presumed to determine the binding energies within the MT structure and hence its overall stability. Fig. 9 shows the neighborhood of a selected tubulin dimer in the MT lattice with particular emphasis on the differences between the dimer-dimer contacts for the isotypes studied in this article. Fig. 9 *a* shows the $\alpha\beta_{III}$ and Fig. 9 *b* shows the $\alpha\beta_{IV}$ structure. Red stick residues are the differences within the isotypes that occur on the tubulin surface. The adjacent monomers are colored pink for α-values and blue for βs. The α-values that make up the intradimer interface are at the bottom of the image and the α-values that make up the interdimer interface are at the top. The yellow surfaces are those residues that interact with isotype differences within a 6 Å cutoff. We have also labeled these residues in the figures as blue text. The residues within the β-isotypes that interact with adjacent monomers are labeled in yellow text, with the appropriate $\alpha\beta_{II}$ to $\alpha\beta_{III}$ or $\alpha\beta_{IV}$ substitution indicated. Within the $\alpha\beta_{III}$ isotype, the residues that interact with the α at the bottom might interfere with dimer assembly itself. These images indicate that the interdimer bonds in the tubulin isotype structures are affected by their different residue composition and hence may explain the differences in the observed assembly/disassembly dynamics although direct demonstration requires a Brownian dynamics simulation to be performed.

CONCLUSIONS

This article has been concerned with an analysis of assembly and disassembly data for individual MTs composed of the purified tubulin isotypes $\alpha\beta_{II}$, $\alpha\beta_{III}$, $\alpha\beta_{IV}$, and for mixtures of tubulin isotypes. The approach adopted here has been based mainly on recursive maps for the data points, to augment the customary representation in the form of time series. The major advantage is the simplicity of the mathematical formulas used in simulations. The models presented here possess sufficient flexibility and can be easily extended to capture a number of subtle features such as: 1), catastrophe events; 2), memory effects; 3), saturation of growth; and 4), the presence of the attenuation state amid both growing and shortening phases. We conclude that the rather simple-minded simulations of assembly and disassembly processes of individual MTs which have been presented in this article are capable of successfully reproducing many of the characteristic features of the experimental data available in the literature. Admittedly, all the models described here are one-dimensional and hence do not properly reflect such features as the number of protofilaments, the overall shape of the growing tip, structural defects, and the role of internal degrees of freedom (for example, different tubulin conformations or hydrolysis energy). However, we believe that these additional features can be successfully incorporated at a later stage by further developing and extending the one-dimensional model.

The analysis of the previously reported data and the data presented here for the first time (to our knowledge) has provided us with a number of very interesting insights into the assembly/disassembly process.

First, it appears that despite varying degrees of dynamicity, the three different β-tubulin isotypes studied have virtually identical growth rates and the only differences seen pertain to the rescue frequencies, albeit they are subtle. We have pointed out some structural differences between the isotypes, mainly at the dimer-dimer interface, which may indeed explain why the catastrophe rates differ among them. A full molecular dynamics simulation of this process has not

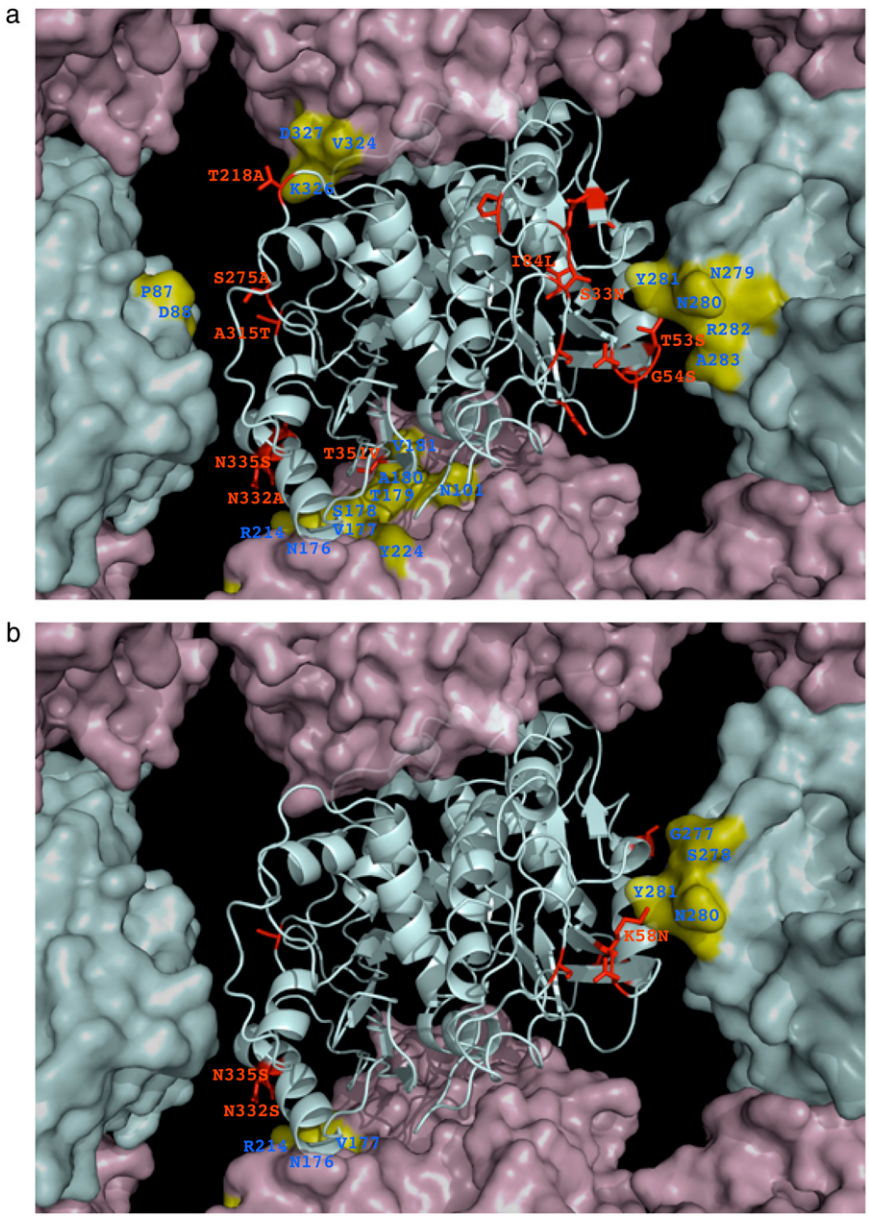

FIGURE 9 Panel *a* shows a fragment of the $\alpha\beta_{III}$ while panel *b* shows the $\alpha\beta_{IV}$ microtubule. Red stick residues are the differences within the isotypes that occur on the tubulin surface. The adjacent monomers are colored pink for α-values and blue for β-values. The α-values that make up the intradimer interface are at the bottom of the image and the α-values that make up the interdimer interface are at the top. The yellow surfaces are those residues that interact with isotype differences within a six-angstrom cutoff. These residues are labeled in blue text. The residues within the β-isotypes that interact with adjacent monomers are labeled in yellow text, with the appropriate $\alpha\beta_{II}$ to $\alpha\beta_{III}$ to $\alpha\beta_{IV}$ substitutions indicated. Within the $\alpha\beta_{III}$ isotype, the residues that interact with the α-values at the bottom might interfere with dimer assembly itself.

been accomplished yet due to huge computational demands but it may one day clarify the issue quantitatively.

The second observation made through our data analysis is that the inherent fluctuation rates in the growing and shortening rates may indeed be linked to the microscopic nature of the GTP-state at the MT tip. We found that $\alpha\beta_{II}$ and $\alpha\beta_{IV}$ isotypes are similar in this respect, while $\alpha\beta_{III}$ differs. To be precise, if the plus-end of a microtubule made up of $\alpha\beta_{II}$, $\alpha\beta_{III}$, or $\alpha\beta_{IV}$ tubulin has nine or more GTP molecules at the available exchangeable guanine nucleotide binding sites, the MT will grow. However, if the MT has eight GTPs, then it will grow if it is made up of $\alpha\beta_{II}$ or $\alpha\beta_{IV}$ tubulin, but it will be in the attenuation state if it is made up of $\alpha\beta_{III}$ tubulin. Conversely, if the plus-end of a microtubule made up of $\alpha\beta_{II}$, $\alpha\beta_{III}$, or $\alpha\beta_{IV}$ tubulin has four or fewer GTPs, then the MT is likely to shorten. However, if the MT end has five GTPs, then a microtubule made up of $\alpha\beta_{II}$ or $\alpha\beta_{IV}$ tubulin will be in the attenuation state, while a microtubule made up of $\alpha\beta_{III}$ tubulin will shorten; i.e., the dependence of the dynamic behavior of MTs on the GTP/GDP ratio at the plus-end is isotype-dependent. In other words, one could imagine, assuming that this ratio is dependent on the GTP concentration in the cell, that MTs made up of $\alpha\beta_{III}$, compared to MTs made from the other dimers, will be less likely to grow and more likely to shorten as GTP concentration decreases; i.e., a cell could control the dynamic behavior of its MTs by varying the expression of the different tubulin isotypes as well as the GTP concentration. In all cases, if our hypothesis is borne out by further experimental verification, the growing tip may have an in-

complete number of GTP molecules in the exchangeable sites of exposed tubulin dimers resulting in the associated differences in the potential energy barrier and hence different assembly rates. The same can be said about a shortening state and the number of GDP molecules occupying the exchangeable sites.

Third, our results indicate a nonlinear dependence on the concentration values for the contributing isotypes in MTs formed from mixtures of tubulin isotypes. We have fitted the data appropriately and concluded that the most logical explanation of this nonlinear dependence is a differential affinity between tubulin dimers coming from different isotype pools. More specifically, when assembling into a microtubule, identical isotypes have a lesser affinity for forming clusters with each other than do different isotypes. The concept of isotype clustering raises the possibility of some highly subtle and complex regulatory phenomena. For example, the fact that a mixture of $\alpha\beta_{\mathrm{II}}$ and $\alpha\beta_{\mathrm{III}}$ generates a microtubule whose dynamic properties are outside of the range defined by those of the two isotypes individually, means that the range of dynamic properties available to a cell is greater than that which would be available if the dynamic properties of a mixed MT were linearly dependent on the relative amounts of the two isotypes. One could imagine that having a wider range of possible MT dynamic behaviors would be advantageous to the cell.

Also, the observation that one dimer can influence the dynamic properties of another one (in particular binding to an MT) is highly intriguing. This raises the possibility that one dimer can induce conformational changes that affect other dimers including possibly dimers that are not immediately adjacent to the first one. Such a phenomenon could have more implications than just dynamics. For instance, binding of other proteins, such as motors, to the MT, could be spaced as a result of this conformational change. Such a phenomenon was first proposed for the heliozoan axopodium by Roth et al. (23,24). They postulate that a ligand binding to one tubulin molecule in a microtubule could cause a graded conformational change that would inhibit binding of another molecule of that ligand to adjacent tubulin molecules. The change would dissipate with increasing distance from the ligand, allowing a tubulin molecule at an appropriate distance from the first one to bind to another molecule of that ligand as well. That is, there would be even spacing among the ligand molecules. Our results are consistent with such a model. In practical terms, the β_{II}, β_{IVa}, β_{Ivb}, and β_{I} isotypes may be too similar to each other to exhibit very complex clustering properties (although this has not yet been tested), so cells whose tubulin expression is limited to these isotypes may not exhibit the effects of clustering that we have hypothesized. However, the differences between these isotypes, and β_{III} and β_{V}, are substantially greater and cells containing at least one of the latter two isotypes, as well as some of the former, would show clustering and may indeed exhibit the hypothesized effects.

To further test our model, it would be interesting to conduct experimental assays with more than two tubulin isotypes present. To verify the utility of the recursive map approach, on the other hand, data sets for a single isotype for vastly different tubulin concentrations should be analyzed as they may clarify the origin of the various types of nonlinear terms in the recursive map due to saturation, competition, and nucleation effects.

APPENDIX A: THE BASIC STOCHASTIC MODEL FOR MICROTUBULES

It is clear that the behavior of an individual MT is stochastic. Here, following Bolterauer et al. (39), we briefly review a stochastic model for MTs. In general, the key reactions of a microtubule during growing/shortening phases can be summarized as

$$\begin{aligned} &M(n)+T\rightarrow M(n+1) && \text{with probability } t_1,\\ &M(n)\rightarrow M(n-1)+T && \text{with probability } t_2,\\ &M(n)\rightarrow M(n-m)+mT && \text{with probability } t_3,\\ &M(n)\rightarrow M(n) && \text{with probability } 1-t_1-t_2-t_3, \end{aligned} \tag{11}$$

where $M(n)$ represents a microtubule composed of n tubulin (T) dimers with length a. As a result, the length of the $MT(n)$ is $\ell(t) = na$. The third reaction describes an incomplete catastrophe, i.e., allows for a rescue event to follow. Here m is a random integer number in the range $0 < m \leq \ell(t)/a$. Note that $m = n$ means there is no rescue during a catastrophe.

The probabilities t_{i} are just the transition rates t_{ri} for a given process multiplied by the probability of finding the reactant molecules in a given reaction region, and thus, for a single MT, are given by

$$\begin{aligned} t_1 &= c_{\mathrm{T}} t_{\mathrm{r1}},\\ t_2 &= t_{\mathrm{r2}},\\ t_3 &= t_{\mathrm{r3}}, \end{aligned} \tag{12}$$

where c_{t} denotes the concentration of tubulin. The connection between the transition rates t_{ri} and the reaction constants k_{i} is

$$t_{\mathrm{ri}} = k_{\mathrm{i}} \Delta t, \tag{13}$$

where Δt is the time step in the simulation. The value r is a random number in the interval $0 \leq r \leq 1$. As a result, a stochastic equation that describes the length evolution $\ell(t)$ as a function of time t for an individual MT can be written as

$$\ell(t+\Delta t) = \begin{cases} \ell(t)+a & \text{for } 0 < r \leq t_1\\ \ell(t)-a & \text{for } t_1 < r \leq t_1+t_2\\ \ell(t)-ma & \text{for } t_1+t_2 < r \leq t_1+t_2+t_3\\ \ell(t) & \text{for } t_1+t_2+t_3 < r \leq 1 \end{cases}. \tag{14}$$

Equation 14 represents the recursive maps that relate length of MTs at time $t + \Delta t$ to time t. Estimating various associated averaged quantities for an ensemble of MTs with different lengths requires a knowledge about the probability distribution $P(n,t)$ that characterizes the system in a given state n at a time t. To calculate $P(n,t)$, one needs to know the transition probabilities for the processes leading into the given state n (i.e., rate in), and the processes leading out of state n and into any other possible state (i.e., rate out). Furthermore, these probabilities t_{ri} are simply proportional to the reaction rates k_{i} (see Eq. 13). In general, a master equation is written as

$$\frac{d}{dt}P(n,t) = (\text{rate in}) - (\text{rate out}). \tag{15}$$

For our reaction scheme in Eq. 11, the master equation becomes

$$\begin{aligned}\frac{d}{dt}P(n,t) = {} & c_{\mathrm{T}}t_{\mathrm{r1}}P(n-1,t) + t_{\mathrm{r2}}P(n+1,t) \\ & + t_{\mathrm{r3}}\sum_{\mathrm{m}=1}^{\infty} w(n,m)P(n+m,t) \\ & - (c_{\mathrm{T}}t_{\mathrm{r1}} + t_{\mathrm{r2}} + t_{\mathrm{r3}})P(n,t)\end{aligned} \tag{16}$$

for $n > 0$. The value $w(n,m)$ is the probability that a collapsing MT of length $n + m$ is rescued at length n. For evenly distributed rescue probability we have

$$w(n,m) = \frac{1}{n}. \tag{17}$$

The master equation for $n = 0$ follows again from Eq. 15, but it also ensures the time independence of the norm $\sum_{\mathrm{n}=0}^{\infty}P(n,t) = 1$ and has the form

$$\frac{d}{dt}P(0,t) = t_{\mathrm{r2}}P(1,t) + t_{\mathrm{r3}}\sum_{\mathrm{n}=1}^{\infty}P(n,t) - c_{\mathrm{T}}t_{\mathrm{r1}}P(0,t). \tag{18}$$

Note that collapsing to $n = 0$ state from an n state means that no rescue occurs in the process. The steady-state equation, that is, $(d/dt)P(n,t) = 0$, can be solved with respect to the normalization condition $\sum_{\mathrm{n}=0}^{\infty}P(n,t) = 1$. It is straightforward to take the continuum limit of the master equation. This is done by expanding the probability $P(n \pm 1,t)$ as follows:

$$P(n\pm 1,t) \rightarrow P(x,t) \pm \frac{\partial}{\partial x}P(x,t) + \frac{1}{2}\frac{\partial^2}{\partial x^2}P(x,t) \pm \ldots. \tag{19}$$

Expanding Eq. 16 up to the first-order terms, one finds

$$\begin{aligned}\frac{\partial}{\partial t}P(x,t) = {} & -(c_{\mathrm{T}}t_{\mathrm{r1}} - t_{\mathrm{r2}})\frac{\partial}{\partial x}P(x,t) - t_{\mathrm{r3}}P(x,t) \\ & + t_{\mathrm{r3}}\int_{\mathrm{x}}^{\infty} w(x')P(x',t)dx',\end{aligned} \tag{20}$$

where x is the continuum limit equivalent of n. For evenly distributed rescue events, i.e., $w(x) = 1/x$, Eq. 20 has the stationary solution as

$$P(x)\text{: } x\, e^{-\frac{t_{\mathrm{r3}}}{c_{\mathrm{T}}t_{\mathrm{r1}} - t_{\mathrm{r2}}}x}, \tag{21}$$

which is, in fact, a bell-shaped solution. The uniform probability distribution assumption for rescues is highly limiting and, hence, may result in solutions that are not appropriate for all experimentally observed situations.

APPENDIX B: EXTENSIONS OF THE STOCHASTIC MODEL

A more detailed description of the models presented below can be found in Tuszynski et al. (40), where additional numerical examples are shown to help the reader better understand the concepts proposed. The first natural extension of the basic model presented in Appendix A introduces incomplete catastrophes, which means that a given MT may exhibit a rapid shortening to a fraction of its previous length. One of the simplest iterative maps to reflect this property is

$$\ell(n+1) = rc(\ell(n) + b) + (1-r)e(\ell(n) + d). \tag{22}$$

The first term in the equation above describes growth (for $r = 1$) at a rate bc over the time unit while the second describes shortening (for $r = 0$) to the length $e\,\ell(n)$ with a growth increment d. We assume that $b > d$ and $c > e$. The length histogram is not affected by this assumption.

To generate saturation characteristics of the growth phase, a simple addition is needed in the recursive equation above that will effectively stop the growth of MTs whose length exceeds a particular upper bound. The first such possibility makes use of a nonlinear term,

$$\ell(n+1) = rc(\ell(n) + b) + (1-r)e(\ell(n) + d) - f\ell^2(n), \tag{23}$$

where $f > 0$ will ensure saturation (as opposed to an unbounded growth for $f < 0$). The second model simply reduces the growth step per time-unit according to a linear dependence of the used tubulin that is proportional to the length of the MT itself,

$$\ell(n+1) = r(\ell(n) + a - f\ell(n)). \tag{24}$$

Again $f > 0$ will ensure the emergence of saturation that will lead to a termination of the MT growth. In the third variant of this model, the reduction of the growth step per time unit is generated through the introduction of the attenuation states whose probability is length-dependent. Averaging over a couple of time steps the growth rate becomes also length-dependent. The model includes now two random numbers r_1 that determine the occurrence of catastrophes and r_2 growth and the attenuation states, respectively. The number $r_1 = 1$ with probability p_1, else 0, and $r_2 = 1$ with probability is

$$\begin{aligned}& p_2[\ell(n)] = p_2(0)(\max - \ell(n))/\max, \\ & \text{else } 0.\end{aligned} \tag{25}$$

In all models of this type the length histogram is only marginally affected. There is a saturation cutoff for long MTs, but in the short range the exponential distribution is still correct to a very good approximation.

Another simple extension of the model is capable of capturing the presence of the attenuation states in the system. We add to the model another random number such that, in addition to a growth stage (with a probability p_1p) and catastrophe (with a probability q), the attenuation state could take place (with a probability p_2p). With no other processes allowed this implies that

$$(p_1 + p_2)p + q = p + q = 1, \tag{26}$$

and a simple return map equation can be written in the form

$$\ell(n+1) = r_1(\ell(n) + ar_2), \tag{27}$$

where r_1 is the first random number (valued 1 for growth for the attenuation state with a probability p while 0 for a catastrophe with a probability q) and r_2 is the second random number (valued 1 for growth with a probability p_1 and 0 for the attenuation state with a probability p_2). The resultant statistical description is somewhat more involved compared to the basic model. The probability of a particular sequence of n_1 growth steps and n_2 the attenuation states such that we have $n = n_1 + n_2$ time steps before a catastrophe is given by

$$P(n_1,n_2) = Aq^2p^{(\mathrm{n}_1+\mathrm{n}_2)}(n_1+n_2)!n_1!n_2!p_1^{\mathrm{n}_1}p_2^{\mathrm{n}_2}. \tag{28}$$

This yields, by summation over all the possible attenuation states, to the length distribution of

$$P(n_1) = Aq^2(pp_1)^{\mathrm{n}_1}n_1!\sum_{\mathrm{n}_2}^{\infty}(n_1+n_2)!n_2!(pp_2)^{\mathrm{n}_2}. \tag{29}$$

The authors thank Dr. Michael Hendzel for his insightful comments and Ms. Kristy Beinert and Mr. Joe Senez for their assistance in the preliminary data analysis. The use of the resources of the Laboratory of Dr. Leslie Wilson at the University of California at Santa Barbara is gratefully acknowledged.

This research was supported by the Natural Sciences and Engineering Research Council of Canada, the Allard Foundation, the United States

Army, Canadian Space Agency, and the Alberta Cancer Board, as well as the following grants to R.F.L.: grant No. W81XWH-05-1-0238 from the Department of Defense Breast Cancer Research Program, grant No. P30 CA54174 from the San Antonio Cancer Institute, a grant from the Texas Higher Education Coordinating Board; and to M.A.J., National Institutes of Health grant No. CA57291.

REFERENCES

1. Dustin, P. 1984. Microtubules, 2nd Ed. Springer, Berlin.
2. Alberts, B., J. Lewis, M. Raff, K. Roberts, and J. D. Watson. 1994. Molecular Biology of the Cell. Garland, New York.
3. Mitchison, T., and M. Krischner. 1984. Microtubule assembly nucleated by isolated centrosomes. *Nature*. 312:232–236.
4. Rezania, V., and J. A. Tuszynski. 2007. From a quantum mechanical description of the assembly processes in microtubules to their semiclassical nonlinear dynamics. *Quantum Biosys.* 1:1–20.
5. Erickson, H. P., and T. E. O'Brien. 1992. Microtubule dynamic instability and GTP hydrolysis. *Annu. Rev. Biophys. Biomol. Struct.* 21: 145–166.
6. Caplow, M., R. L. Ruhlen, and J. Shanks. 1994. The free energy for hydrolysis of a microtubule-bound nucleotide triphosphate is near zero: all of the free energy for hydrolysis is stored in the microtubule lattice. *J. Cell Biol.* 127:779–788.
7. Mandelkow, E.-M., and E. Mandelkow. 1992. Microtubule oscillations. *Cell Motil. Cytoskeleton.* 22:235–244.
8. Trinczek, B., A. Marx, E.-M. Mandelkow, B. D. Murphy, and E. Mandelkow. 1993. Dynamics of microtubules from erythrocyte marginal bands. *Mol. Biol. Cell.* 4:323–335.
9. Fygenson, D. K., H. Flyvbjerg, K. Sneppen, A. Libachaber, and S. Leibler. 1995. Spontaneous nucleation of microtubules. *Phys. Rev. E.* 51:5058–5063.
10. Cassimeris, L., N. K. Pryer, and E. D. Salmon. 1988. Real-time observations of microtubule dynamic instability in living cells. *J. Cell Biol.* 107:2223–2231.
11. Drechsel, D. N., A. A. Hyman, M. H. Cobb, and M. W. Kirschner. 1992. Modulation of dynamic instability of microtubule assembly by the microtubule associated protein tau. *Mol. Biol. Cell.* 3:1141–1154.
12. Wordeman, L., and T. J. Mitchison. 1994. Dynamics of microtubule assembly in vivo. *In* Microtubules. C. Lloyd and J. Hyams, editors. Wiley, New York.
13. McIntosh, R. 1994. The role of microtubules in chromosome movement. *In* Microtubules. C. Lloyd and J. Hyams, editors. Wiley, New York.
14. Panda, D., H. P. Miller, A. Banerjee, R. F. Luduena, and L. Wilson. 1994. Microtubule dynamics in vitro are regulated by the tubulin isotype composition. *Cell Biol.* 91:11358–11362.
15. Derry, W. B., L. Wilson, I. A. Khan, R. F. Luduena, and M. A. Jordan. 1997. Taxol differentially modulates the dynamics of microtubules assembled from unfractionated and purified β-tubulin isotypes. *Biochemistry.* 36:3554–3562.
16. Lu, Q., and R. Luduena. 1994. In vitro analysis of microtubule assembly of isotypically pure tubulin dimers. Intrinsic differences in the assembly properties of $\alpha\beta_{II}$, $\alpha\beta_{III}$, and $\alpha\beta_{IV}$ tubulin dimers in the absence of microtubule-associated proteins. *J. Biol. Chem.* 269:2041–2047.
17. Carpenter, E. J., J. Torin Huzil, R. F. Luduena, and J. A. Tuszynski. 2006. Homology modeling of tubulin: influence predictions for microtubules biophysical properties. *Eur. J. Biophys.* 36:35–43.
18. Luduena, R. 1998. Multiple forms of tubulin: different gene products and covalent modifications. *Int. Rev. Cytol.* 178:207–275.
19. Ngan, V. K., K. Bellman, D. Panda, B. T. Hill, M. A. Jordan, and L. Wilson. 2000. Novel actions of the antitumor drugs Vinflunine and Vinorelbine on microtubules. *Cancer Res.* 60:5045–5051.
20. Panda, D., H. Miller, and L. Wilson. 1999. Rapid treadmilling of brain microtubules free of microtubule-associated proteins in vitro and its suppression by tau. *Proc. Natl. Acad. Sci. USA.* 96:12459–12464.
21. Schek, H. T., M. K. Gardner, J. Cheng, D. J. Odde, and A. J. Hunt. 2007. Microtubule assembly dynamics at the nanoscale. *Curr. Biol.* 17: 1445–1455.
22. Banerjee, A., M. C. Roach, P. Trcka, and R. F. Luduena. 1992. Preparation of a monoclonal antibody specific for the class IV isotype of β-tubulin. Purification and assembly of $\alpha\beta_{II}$, $\alpha\beta_{III}$, and $\alpha\beta_{IV}$ tubulin dimers from bovine brain. *J. Cell Biol.* 267:5625–5630.
23. Roth, L. E., D. J. Pihlaja, and Y. Shigenaka. 1970. Microtubules in the heliozoan axopodium. I. The gradion hypothesis of allosterism in structural proteins. *J. Ultrastruct. Res.* 30:7–37.
24. Roth, L. E., and D. J. Pihlaja. 1977. Gradionation: hypothesis for positioning and patterning. *J. Protozool.* 24:2–9.
25. Flyvbjerg, H., T. E. Holy, and S. Leibler. 1996. Microtubule dynamics: caps, catastrophes, and coupled hydrolysis. *Phys. Rev. E.* 54:5538–5560.
26. Panda, D., H. P. Miller, and L. Wilson. 2002. Determination of the size and chemical nature of the stabilizing ''cap'' at microtubule ends using modulators of polymerization dynamics. *Biochemistry.* 41:1609–1617.
27. Odde, D. J., L. Cassimeris, and H. M. Buettner. 1995. Kinetics of microtubule catastrophe assessed by probabilistic analysis. *Biophys. J.* 69:796–802.
28. Williams, R. 2002. Concentration dependence of variability in growth rate of microtubules. *Biophys. J.* 83:1809–1819.
29. Janson, M. E., and M. Dogterom. 2004. A bending mode analysis for growing microtubules: evidence for a velocity-dependent rigidity. *Biophys. J.* 87:2723–2736.
30. Hill, T. L., and M. W. Kirschner. 1982. Bioenergetics and kinetics of microtubule and actin filament assembly-disassembly. *Int. Rev. Cytol.* 78:1–125.
31. Bayley, P. M., M. J. Schilstra, and S. R. Martin. 1989. A simple formulation of microtubule dynamics: quantitative implications of the dynamic instability of microtubule populations in vivo and in vitro. *J. Cell Sci.* 93:241–254.
32. Bayley, P. M., M. J. Schilstra, and S. R. Martin. 1990. Microtubule dynamic instability: numerical simulation of microtubule transition properties using a lateral cap model. *J. Cell Sci.* 95:33–48.
33. Martin, S. R., M. J. Schilstra, and P. M. Bayley. 1993. Dynamic instability of microtubules: Monte Carlo simulation and application to different types of microtubule lattice. *Biophys. J.* 65:578–596.
34. Amos, L. A. 1995. The microtubule lattice—20 years on. *Trends Cell Biol.* 5:48–51.
35. Horio, T., and H. Hotani. 1986. Visualization of the dynamic instability of individual microtubules by dark-field microscopy. *Nature.* 321: 605–607.
36. Mandelkow, E., and E.-M. Mandelkow. 1994. Microtubule structure. *Curr. Opin. Struct. Biol.* 4:171–179.
37. Walker, R. A., N. K. Pryer, and E. D. Salmon. 1991. Dilution of individual microtubules observed in real time in vitro: evidence that cap size is small and independent of elongation rate. *J. Cell Biol.* 114: 73–81.
38. Flyvbjerg, H., T. E. Holy, and S. Leibler. 1994. Stochastic dynamics of microtubules: a model for caps and catastrophes. *Phys. Rev. Lett.* 73: 2372.
39. Bolterauer, H., H.-J. Limbach, and J. A. Tuszynski. 1999. Models of assembly and disassembly of individual microtubules: stochastic and averaged equations. *J. Biol. Phys.* 25:1–22.
40. Tuszynski, J. A., D. Sept, H. Bolterauer, and H.-J. Limbach. 1998. Stochastic data analysis for the assembly and disassembly of microtubules in vitro. *Adv. Structural Biol.* 5:169–201.
41. Tuszynski, J. A., E. Carpenter, J. Torin, J. Huzil, W. Malinski, T. Luchko, and R. F. Luduena. 2006. The evolution of the structure of tubulin and its potential consequences for the role and function of microtubules in cells and embryos. *Int. J. Dev. Biol.* 50:341–358.